Signal Processing 238 (2026) 110086

Contents lists available at ScienceDirect

Signal Processing

journal homepage: www.elsevier.com/locate/sigpro

Optimized sparse 2D antenna array design via beampattern matching☆

Saeid Sedighi [a], Nazila Karimian-Sichani [b,*], Bhavani Shankar M.R. [c], Maria S. Greco [b], Fulvio Gini [b], Björn Ottersten [c]

[a] Valeo Schalter und Sensoren GmbH, Germany
[b] Department of Information Engineering, University of Pisa, Pisa, Italy
[c] Interdisciplinary Centre for Security, Reliability and Trust (SnT), University of Luxembourg, Luxembourg

ARTICLE INFO

Keywords:
Array configuration
Beampattern optimization
Sparse array
MIMO radar
Antenna placement
Planar array

ABSTRACT

Emerging millimeter-wave (mmWave) MIMO radars combine the benefits of large bandwidth available at mmWave frequencies with the spatial diversity provided by MIMO architectures, significantly enhancing radar capabilities for automotive, surveillance, and imaging applications. However, deploying large numbers of antennas and transceivers at these high frequencies substantially increases chip complexity and hardware costs. In this paper, we address the design of sparse two-dimensional (2D) antenna arrays that retain the desirable beampattern characteristics of fully populated arrays – namely, narrow mainlobes and low sidelobes – while significantly reducing the required number of antenna elements. We formulate the sparse array design problem as a beampattern matching optimization, which selects optimal subsets of transmit and receive antenna positions from an initial dense grid. To efficiently solve this challenging nonconvex optimization problem, we introduce an iterative algorithm combining Majorization–Minimization (MM) and Alternating Optimization (AO) techniques. We provide theoretical guarantees for convergence to at least a local optimum. Additionally, we propose a weighting vector optimization step to further enhance sidelobe suppression. Numerical simulations confirm that the proposed method maintains angular resolution and Sidelobe Levels (SLLs) comparable to those of full arrays, while substantially reducing hardware complexity and cost. Performance comparisons against existing methods demonstrate notable improvements in sidelobe suppression and computational efficiency without compromising processing gain.

1. Introduction

Multiple-input multiple-output (MIMO) radar has emerged as a powerful technology, significantly enhancing radar performance through improved target detection, localization, and tracking capabilities [1,2]. Utilizing multiple transmitting and receiving antennas, MIMO radar systems exploit spatial diversity, resulting in superior resolution and parameter estimation accuracy. The recent advancement of millimeter-wave (mmWave) technologies has further accelerated these capabilities, combining the substantial available bandwidth at mmWave frequencies with the inherent spatial diversity offered by MIMO architectures. Consequently, mmWave MIMO radars have demonstrated unprecedented performance advantages, making them particularly appealing for automotive radar, surveillance, and high-resolution imaging applications [3].

A critical aspect of mmWave MIMO radar systems is the antenna array design, which inherently involves a trade-off between system performance, cost, and complexity. Fully populated antenna arrays, characterized by densely arranged antennas spaced uniformly at half-wavelength intervals and supported by dedicated transceivers, achieve excellent spatial resolution and beamforming capabilities. However, their practical deployment is often limited by high hardware costs, substantial power consumption, and complex signal processing requirements. To address these challenges, Sparse Antenna Arrays (SAAs) have gained considerable attention due to their reduced complexity, lower hardware costs, and improved energy efficiency [4]. Nevertheless,

☆ This work has been partially supported by the Luxembourg National Research Fund (FNR) under the projects C20/IS/14799710/SENCOM, INTER/MOBILITY/2023/IS/18014377/MCR, and the Italian Ministry of Education and Research (MUR) in the framework of the FoReLab project (Departments of Excellence).

* Corresponding author.
E-mail address: Nazila.karimian@ing.unipi.it (N. Karimian-Sichani).

https://doi.org/10.1016/j.sigpro.2025.110086
Received 16 October 2024; Received in revised form 28 March 2025; Accepted 1 May 2025
Available online 21 May 2025

sparse array designs must be carefully optimized to avoid degrading spatial resolution or inadvertently increasing SLLs.

1.1. Related works

The design and optimization of sparse antenna arrays for mmWave MIMO radar have been extensively studied, and existing works can be categorized based on the dimensionality of the arrays (1D or 2D) and their respective optimizationobjectives [5–24]. In the context of one-dimensional (1D) SAAs, joint optimization of waveform covariance matrices and antenna positions for transmit beampattern matching was explored in [7,10]. Specifically, [7] developed an iterative algorithm to minimize the mean-square error (MSE) between designed and desired transmit beampatterns. On the other hand, the work in [10] extends this idea by not only minimizing the transmit beampattern matching error but also integrating additional constraints to enable flexible control of the beampattern characteristics within predefined angular regions, including mainlobe ripple and peak SLLs. Furthermore, the authors in [11] proposed a sparse antenna design method exploiting the relationship between diagonal elements of the optimized waveform covariance matrix and transmitted antenna power, retaining only antennas significantly contributing to the desired beampattern. Joint transmit-receive beampattern optimization for 1D sparse array design was studied in [6,8]. A genetic algorithm was employed in [6] to optimize Sparse Linear Array (SLA) configurations for enhanced direction-of-arrival (DOA) estimation in multistatic scenarios. The authors in [8] developed a two-step synthesis procedure tailored for 3D imaging radar, significantly reducing the number of antenna elements while maintaining angular resolution and effectively suppressing SLLs. Moreover, the Cramer–Rao lower bound (CRLB) was employed as a metric in joint antenna and pulse placement designs to minimize hardware complexity and energy consumption without sacrificing accuracy [9,12]. Recently, convolutional neural networks (CNNs) were leveraged in [23] for optimal SLA design aimed at improved DOA estimation.

Despite the substantial research on 1D SSA designs, fewer works have addressed two-dimensional (2D) configurations. The authors in [18] introduced an optimization framework for designing 2D MIMO virtual arrays, employing an iterative coordinate descent algorithm to minimize the MSE between the designed and desired virtual arrays under constraints on the number of transmit and receive antennas.

However, existing research has not yet simultaneously addressed key performance metrics such as mainlobe resolution, sidelobe suppression, and processing gain within the context of sparse 2D antenna array design. To bridge this gap, we formulate and solve the 2D SAA design problem, explicitly considering mainlobe resolution, sidelobe level, processing gain, and array flexibility for a given sparsity order. Our approach is designed for offline application, facilitating the manufacturing of optimized antenna arrays and associated chip designs without the need for subsequent reconfiguration.

1.2. Contribution of this paper

Motivated by these research gaps, this paper proposes an SAA design for mmWave MIMO radars with 4D imaging capabilities, considering both transmit and receive beampattern characteristics. The main contributions of this paper are as follows:

- We formulate the joint transmit and receive beampattern matching optimization problem for 2D SAAs with predefined numbers of transmit and receive elements. By employing binary transmit and receive array position vectors, we design arrays that achieve specified beampattern characteristics with significantly reduced SLLs while preserving the mainlobe resolution comparable to fully populated arrays.
- To solve the resulting non-convex NP-hard discrete optimization problem, we propose a novel iterative algorithm based on the method of majorization–minimization (MM) and an alternating optimization (AO) approach. We provide theoretical guarantees for convergence to at least a local optimum, ensuring algorithm robustness and stability.
- We integrate a weighting vector optimization into the array design process, adding flexibility and further enhancing the array's beampattern quality, particularly in sidelobe suppression.
- Comprehensive numerical evaluations demonstrate that our proposed algorithm achieves the required angular resolution, low sidelobe performance and processing gain despite substantial antenna sparsity.

1.3. Organization and notation

The rest of this paper is organized as follows: Section 2 formulates the antenna array design problem. Section 3 details the proposed optimization algorithm. Section 4 discusses the enhancement of the designed array's beampattern through a weighting vector optimization. Simulation results validating our method are presented in Section 5. Finally, Section 6 concludes the paper.

Notation: We use boldface upper case $\mathbf{X}$ for matrices and boldface lower case $\mathbf{x}$ for vectors. ln(.), and mod(.) and vec(.) define the natural logarithm, reminder and vectorization operator, respectively. $\|.\|_F$, $\|.\|_0$ and $\|.\|_1$ and $\|.\|_2$ are the Frobenius, Zero, Manhattan and Euclidean norm, respectively. Also, the transpose and Hermitian operators are denoted by $(.)^T$ and $(.)^H$, respectively. $|x|$ denotes modulus of the complex number x and $|\mathbf{x}|$ is a vector of element wise absolute values of $\mathbf{x}$, i.e., $|\mathbf{x}| = \left[|x_1|, |x_2|, \dots, |x_L|\right]^T$. $\mathbb{R}^N$ and $\mathbb{C}^N$ are the N-dimensional real and complex vector spaces. $\mathbf{X} \succeq 0$ denotes the matrix $\mathbf{X}$ is positive semidefinite. $\mathbf{I}_N$ is a $N \times N$ Identity matrix. The Hadamard product, Kronecker product, gradient and floor function are denoted by $\odot$, $\otimes$, ∇ and $\lfloor . \rfloor$, respectively.

2. Problem formulation for 2D sparse antenna array design

In this section, we define the system model and formulate the problem of designing 2D SAAs for MIMO radar. Specifically, we consider a colocated MIMO radar system, where multiple transmit and receive antennas are closely spaced, enabling coherent signal processing. We assume that each transmit antenna is assumed to emit an orthogonal waveform, ensuring negligible cross-correlation between the received signals, thereby decoupling the array's spatial beampattern design from the transmitted waveform design. Additionally, antenna coupling effects are assumed to be sufficiently weak and thus negligible. If, however, coupling effects become significant, their impact can be measured through calibration to obtain a coupling matrix, which can subsequently be used to compensate and effectively mitigate the coupling effects on the array beampattern. Thus, even arrays designed under ideal (uncoupled) assumptions can closely achieve their theoretical performance specifications in practical scenarios.

Our objective is to achieve predefined angular resolutions in both azimuth and elevation dimensions while ensuring the SLLs remain below a specified threshold, using a constrained number of transmit and receive antenna elements. To meet these performance criteria, we formulate the array design as an optimization problem. In particular, our goal is to approximate the mainlobe characteristics of a reference 2D fully populated uniform rectangular array (FPURA), which inherently provides the desired angular resolutions, while simultaneously constraining the SLLs and the number of antenna elements.

Let $\Gamma(\theta, \phi)$ denote the normalized array beampattern of a 2D FPURA (shown in Fig. 1(a)) with half-wavelength spacing, i.e., $d = \lambda/2$, where λ is the wavelength. The azimuth and elevation angles are denoted by $\theta \in \boldsymbol{\Theta} = [-90°, 90°]$ and $\phi \in \boldsymbol{\Phi} = [-90°, 90°]$, respectively. In addition, let $L = L_1 \times L_2$ represent the total number of elements in

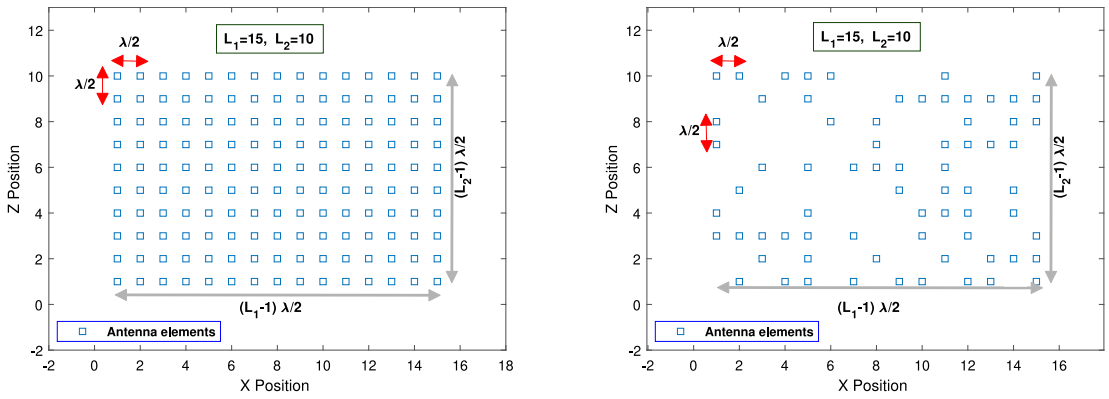

Fig. 1. Configuration and positions of (a): a dense and (b): a sparse array antennas.

the 2D FPURA, with L_1 and L_2 being the number of elements along the azimuth and elevation dimensions, respectively (see Fig. 1). The transmitter and receiver array steering vectors are denoted by $\mathbf{a}_t(\theta,\phi) \in \mathbb{C}^L$ and $\mathbf{a}_r(\theta,\phi) \in \mathbb{C}^L$, respectively. The lth element of each steering vector is given by

$$\mathbf{a}_{t,l}(\theta,\phi) = \mathbf{a}_{r,l}(\theta,\phi) = \exp(j\pi x \sin(\theta)\cos(\phi) + j\pi z \sin(\phi)), \tag{1}$$

where $x = \mathrm{mod}(l-1, L_1)$, $z = \left\lfloor \frac{l-1}{L_1} \right\rfloor$, and $l \in \{1,2,\ldots,L\}$.

Accordingly, the problem of 2D SSA design can now be formulated as the following optimization problem:

$$\begin{cases} \min\limits_{\mathbf{p}_t,\mathbf{p}_r} & \sum\limits_{\substack{\theta\in\Theta_m \\ \phi\in\Phi_m}} \left| \dfrac{\mathbf{a}_t^T(\theta,\phi)\mathbf{p}_t\mathbf{p}_r^T\mathbf{a}_r(\theta,\phi)}{\mathbf{1}_L^T\mathbf{p}_t\mathbf{p}_r^T\mathbf{1}_L} - \Gamma(\theta,\phi) \right|^2 \\ & \|\mathbf{p}_t\|_0 = M, \quad \mathbf{p}_t \in \{0,1\}^L, \\ s.t. & \|\mathbf{p}_r\|_0 = N, \quad \mathbf{p}_r \in \{0,1\}^L, \\ & \left| \dfrac{\mathbf{a}_t^T(\theta,\phi)\mathbf{p}_t\mathbf{p}_r^T\mathbf{a}_r(\theta,\phi)}{\mathbf{1}_L^T\mathbf{p}_t\mathbf{p}_r^T\mathbf{1}_L} \right|^2 \leqslant \mu_1, \quad \forall\theta\in\Theta_s, \phi\in\Phi_s. \end{cases} \tag{2}$$

where Θ_m and Φ_m represent the discrete angular grids in the mainlobe region for the azimuth and elevation angles, while Θ_s and Φ_s denote the corresponding angular grids in the sidelobe region. Vectors $\mathbf{p}_t$ and $\mathbf{p}_r$ are binary arrays that indicate the placement of the transmitter and receiver antennas, respectively. The values of M and N define the number of transmit and receive antennas, and the elements of these vectors are arranged row-wise. Further, μ_1 denotes the desired maximum sidelobe level.

In (2), the objective function seeks to minimize the Euclidean distance between the beampattern of the desired 2D SSA and that of a reference 2D FPURA in the mainlobe region. Further, the first and second constraints ensure that the total number of antennas used is limited to $M \times N$, which is significantly fewer than that in the reference 2D FPURA, i.e., $M \times N \ll L$ (see Fig. 1(b)). The third constraint guarantees that the SLLs do not exceed a predetermined threshold μ_1.

Due to the nonconvexity of the objective function and the binary nature of the optimization variables, this optimization problem is classified as a nonconvex binary optimization problem [25]. In the next section, we present the proposed method for solving this problem.

Remark 1. If the elevation angles ϕ in (2) and the parameter z in transmit and receive array steering vectors in (1) are set to zero, the 2D SSA design Problem in (2) simplifies to a 1D SSA design problem.

3. Solution to the optimization problem

To address the nonconvex binary optimization problem in (2), we start by defining the position vector $\mathbf{p} = [\mathbf{p}_t^T, \mathbf{p}_r^T]^T$, concatenating the transmitter and receiver array position vectors. In addition, we introduce the zero-padded array steering vectors as,

$$\tilde{\mathbf{a}}_t(\theta,\phi) = [\mathbf{a}_t^T, \mathbf{0}_L^T]^T \in \mathbb{C}^{2L}, \tag{3}$$

$$\tilde{\mathbf{a}}_r(\theta,\phi) = [\mathbf{0}_L^T, \mathbf{a}_r^T]^T \in \mathbb{C}^{2L}. \tag{4}$$

Exploiting the constraints $\mathbf{1}_L^T\mathbf{p}_t = M$ and $\mathbf{p}_r^T\mathbf{1}_L = N$, the original objective function in (2) can be reformulated as shown in (7). We also define the auxiliary vectors:

$$\mathbf{e}_t = [\mathbf{1}_L^T, \mathbf{0}_L^T]^T, \tag{5}$$

$$\mathbf{e}_r = [\mathbf{0}_L^T, \mathbf{1}_L^T]^T, \tag{6}$$

which allow us to express the equality constraints from (2) as $\|\mathbf{e}_t \odot \mathbf{p}\|_0 = M$ and $\|\mathbf{e}_r \odot \mathbf{p}\|_0 = N$. Since $\mathbf{e}_t$, $\mathbf{e}_r$, and $\mathbf{p}$ are binary vectors, these constraints are equivalent to $\mathbf{e}_t^T\mathbf{p} = M$ and $\mathbf{e}_r^T\mathbf{p} = N$. With these modifications, the optimization problem becomes:

$$\begin{cases} \min\limits_{\mathbf{p}} & \sum\limits_{\substack{\theta\in\Theta_m \\ \phi\in\Phi_m}} \left| \dfrac{\tilde{\mathbf{a}}_t^T(\theta,\phi)\mathbf{p}\mathbf{p}^T\tilde{\mathbf{a}}_r(\theta,\phi)}{MN} - \Gamma(\theta,\phi) \right|^2 \\ & \mathbf{p} \in \{0,1\}^{2L}, \\ & \mathbf{e}_t^T\mathbf{p} = M, \\ s.t. & \mathbf{e}_r^T\mathbf{p} = N, \\ & \left| \tilde{\mathbf{a}}_t^T(\theta,\phi)\mathbf{p}\mathbf{p}^T\tilde{\mathbf{a}}_r(\theta,\phi) \right|^2 \leqslant (MN)^2\mu, \quad \forall\theta\in\Theta_s, \\ & \qquad\qquad\qquad\qquad\qquad \phi\in\Phi_s. \end{cases} \tag{7}$$

Introducing additional auxiliary variables:

$$\mathbf{Q} \triangleq \mathbf{p}\mathbf{p}^T \in \{0,1\}^{2L\times 2L}, \tag{8}$$

$$\mathbf{E} \triangleq \mathbf{e}_r\mathbf{e}_t^T \in \{0,1\}^{2L\times 2L}, \tag{9}$$

$$\tilde{\mathbf{a}}(\theta,\phi) \triangleq \tilde{\mathbf{a}}_r(\theta,\phi) \otimes \tilde{\mathbf{a}}_t(\theta,\phi) \in \mathbb{C}^{4L^2}, \tag{10}$$

we reformulate the optimization problem as,

$$\begin{cases} \min\limits_{\mathbf{p},\mathbf{Q}} & \sum\limits_{\substack{\theta\in\Theta_m \\ \phi\in\Phi_m}} \left| \dfrac{\tilde{\mathbf{a}}^T(\theta,\phi)vec(\mathbf{Q})}{MN} - \Gamma(\theta,\phi) \right|^2 \\ & \mathbf{p} \in \{0,1\}^{2L}, \\ & \mathbf{e}_t^T\mathbf{p} = M, \\ s.t. & \mathbf{e}_r^T\mathbf{p} = N, \\ & \mathbf{Q} = \mathbf{p}\mathbf{p}^T, \\ & \left| \tilde{\mathbf{a}}^T(\theta,\phi)\mathrm{vec}(\mathbf{Q}) \right|^2 \leqslant (MN)^2\mu_1, \quad \forall\theta\in\Theta_s, \phi\in\Phi_s, \end{cases} \tag{11}$$

Although the objective function is now quadratic and convex, the problem remains nonconvex due to the binary constraint on $\mathbf{p}$ and the

equality constraint $\mathbf{Q} = \mathbf{p}\mathbf{p}^T$. In the following, we present an equivalent reformulation of (11), which paves the way for solving this noconvex optimization problem. To tackle the binary constraint on $\mathbf{p}$, we replace it with:

$$g(\mathbf{p}_i) \triangleq (\mathbf{p}_i - 1)\ln(1-\mathbf{p}_i) - \mathbf{p}_i\ln(\mathbf{p}_i) \leq 0, \tag{12}$$

$$\mathbf{p}_i \in [0,1], \quad \forall i \in \{1,2,\dots,2L\}. \tag{13}$$

It is readily verified that (12) and (13) are satisfied if only if $\mathbf{p}_i = 0$ or 1. Hence, the optimization problem (11) can be rewritten as,

$$\begin{cases} \min\limits_{\mathbf{p},\mathbf{Q},\mathbf{\Lambda},\zeta} & \sum\limits_{\substack{\theta\in\Theta_m \\ \phi\in\Phi_m}} \left| \dfrac{\tilde{\mathbf{a}}^T(\theta,\phi)\mathrm{vec}(\mathbf{Q})}{MN} - \Gamma(\theta,\phi) \right|^2 + \eta_1\zeta \\ & 0 \leqslant \mathbf{p}_i \leqslant 1, \quad \forall i \in \{1,2,\dots,2L\}, \\ & g(\mathbf{p}_i) \leqslant 0, \quad \forall i \in \{1,2,\dots,2L\}, \\ s.t. & \mathbf{e}_t^T\mathbf{p} = M, \\ & \mathbf{e}_r^T\mathbf{p} = N, \\ & \mathbf{Q} = \mathbf{p}\mathbf{p}^T, \\ & \left|\tilde{\mathbf{a}}^T(\theta,\phi)\mathrm{vec}(\mathbf{Q})\right|^2 \leqslant (MN)^2\mu_1, \quad \forall\theta\in\Theta_s, \phi\in\Phi_s, \end{cases} \tag{14}$$

Next, to efficiently handle the challenging equality constraint $\mathbf{Q} = \mathbf{p}\mathbf{p}^T$, we leverage the results provided in [26, Theorem 1] and [5, Theorem 3.1]. Specifically, according to [26, Theorem 1], the equality constraint $\mathbf{Q} = \mathbf{p}\mathbf{p}^T$ is equivalent to imposing a rank-one constraint on the augmented matrix $\mathbf{C}$ defined as,

$$\mathbf{C} = \begin{bmatrix} 1 & \mathbf{p}^T \\ \mathbf{p} & \mathbf{Q} \end{bmatrix} \in [0,1]^{(2L+1)\times(2L+1)}.$$

This rank-one constraint, i.e., $\mathrm{rank}(\mathbf{C}) = 1$, can be equivalently represented by enforcing that all eigenvalue of $\mathbf{C}$, except the largest, are zero. Following [5, Theorem 3.1], this condition can be realized by introducing an auxiliary orthonormal matrix $\mathbf{\Lambda} \in \mathbb{C}^{(2L+1)\times 2L}$, where $\mathbf{\Lambda}^H\mathbf{\Lambda} = \mathbf{I}_{2L}$, and imposing the following constraint:

$$\zeta\mathbf{I}_{2L} - \mathbf{\Lambda}^H\mathbf{C}\mathbf{\Lambda} \succeq 0 \tag{15}$$

where choosing $\zeta \to 0$ ensures that all the eigenvalues of $\mathbf{C}$, except the largest one, approaches zero.[1] Consequently, making use of this reformulation, the optimization problem (14) can now be recast as follows,

$$\begin{cases} \min\limits_{\mathbf{p},\mathbf{Q},\mathbf{\Lambda},\zeta} & \sum\limits_{\substack{\theta\in\Theta_m \\ \phi\in\Phi_m}} \left| \dfrac{\tilde{\mathbf{a}}^T(\theta,\phi)\mathrm{vec}(\mathbf{Q})}{MN} - \Gamma(\theta,\phi) \right|^2 + \eta_1\zeta \\ & 0 \leqslant \mathbf{p}_i \leqslant 1, \quad \forall i \in \{1,2,\dots,2L\}, \\ & g(\mathbf{p}_i) \leqslant 0, \quad \forall i \in \{1,2,\dots,2L\}, \\ & \mathbf{e}_t^T\mathbf{p} = M, \\ & \mathbf{e}_r^T\mathbf{p} = N, \\ s.t. & \left|\tilde{\mathbf{a}}^T(\theta,\phi)\mathrm{vec}(\mathbf{Q})\right|^2 \leqslant (MN)^2\mu_1, \quad \forall\theta\in\Theta_s, \phi\in\Phi_s, \\ & \zeta\mathbf{I}_{2L} - \mathbf{\Lambda}^H\mathbf{C}\mathbf{\Lambda} \succeq 0, \\ & \mathbf{\Lambda}^H\mathbf{\Lambda} = \mathbf{I}_{2L}, \\ & \mathbf{C} \succeq 0, \end{cases} \tag{16}$$

where η_1 is a regularization parameter. This reformulation transforms the original equality constraint into semidefinite constraints suitable for numerical optimization.

[1] A detailed proof of this equivalence is given in [5, Theorem 3.1].

Finally, by introducing a regularization parameter η_2 and moving the constrains $g(\mathbf{p}_i) \leq 0, \quad \forall i \in \{1,2,\dots,2L\}$ to the objective function, the optimization problem (16) can be recast as,

$$\begin{cases} \min\limits_{\mathbf{p},\mathbf{Q},\mathbf{\Lambda},\zeta} & \sum\limits_{\substack{\theta\in\Theta_m \\ \phi\in\Phi_m}} \left| \dfrac{\tilde{\mathbf{a}}^T(\theta,\phi)\mathrm{vec}(\mathbf{Q})}{MN} - \Gamma(\theta,\phi) \right|^2 + \eta_1\zeta + \eta_2\sum\limits_{i=1}^{2L} g(\mathbf{p}_i) \\ & 0 \leqslant \mathbf{p}_i \leqslant 1, \quad \forall i \in \{1,2,\dots,2L\}, \\ & \mathbf{e}_t^T\mathbf{p} = M, \\ & \mathbf{e}_r^T\mathbf{p} = N, \\ s.t. & \left|\tilde{\mathbf{a}}^T(\theta,\phi)\mathrm{vec}(\mathbf{Q})\right|^2 \leqslant (MN)^2\mu_1, \quad \forall\theta\in\Theta_s, \phi\in\Phi_s, \\ & \zeta\mathbf{I}_{2L} - \mathbf{\Lambda}^H\mathbf{C}\mathbf{\Lambda} \succeq 0, \\ & \mathbf{\Lambda}^H\mathbf{\Lambda} = \mathbf{I}_{2L}, \\ & \mathbf{C} \succeq 0. \end{cases} \tag{17}$$

The optimization problem (17) can be solved iteratively by majorizing $g(\mathbf{p}_i)$ and alternating between the optimization variables. Let $\mathbf{p}^{(k)}$, $\mathbf{Q}^{(k)}$, $\mathbf{C}^{(k-1)}$ and $\zeta^{(k)}$ be the values of $\mathbf{p}$, $\mathbf{Q}$, $\mathbf{C}$ and ζ at kth iteration, respectively. Using Majorization-Minimization (MM) technique [27,28], the concave functions $g(\mathbf{p}_i) \quad \forall i \in \{1,2,\dots,2L\}$ in (12) can be majorized by their first-order Taylor expansion as,

$$g(\mathbf{p}_i^{(k)}) \leq h(\mathbf{p}_i^{(k)}) = g(\mathbf{p}_i^{(k-1)}) + \nabla g(\mathbf{p}_i^{(k-1)})(\mathbf{p}_i^{(k)} - \mathbf{p}_i^{(k-1)}), \tag{18}$$

where

$$\nabla g(\mathbf{p}_i) = \ln\frac{1-\mathbf{p}_i}{\mathbf{p}_i} \quad \forall i \in \{1,2,\dots,2L\}. \tag{19}$$

Given $\mathbf{\Lambda}^{(k-1)}$ and $\zeta^{(k-1)}$, the optimization problem with respect to $\mathbf{p}^{(k)}$, $\mathbf{Q}^{(k)}$ and $\zeta^{(k)}$ becomes (20), shown at the top of the next page. The optimization problem (20) is a Semi-Definite Programming (SDP), which can be solved efficiently, e.g. using CVX.

$$\begin{cases} \min\limits_{\mathbf{p^{(k)}},\mathbf{Q^{(k)}},\zeta^{(k)}} & \sum\limits_{\substack{\theta\in\Theta_m \\ \phi\in\Phi_m}} \left| \dfrac{\tilde{\mathbf{a}}^T(\theta,\phi)\mathrm{vec}(\mathbf{Q}^{(k)})}{MN} - \Gamma(\theta,\phi) \right|^2 + \eta_1\zeta^{(k)} + \eta_2\sum\limits_{i=1}^{2L} h(\mathbf{p}_i^{(k)}) \\ & (c1) \quad 0 \leqslant \mathbf{p}_i^{(k)} \leqslant 1, \quad \forall i \in \{1,2,\dots,2L\}, \\ & (c2) \quad \mathbf{e}_t^T\mathbf{p}^{(k)} = M, \\ & (c3) \quad \mathbf{e}_r^T\mathbf{p}^{(k)} = N, \\ s.t. & (c4) \quad \left|\tilde{\mathbf{a}}^T(\theta,\phi)\mathrm{vec}(\mathbf{Q}^{(k)})\right|^2 \leqslant (MN)^2\mu_1, \quad \forall\theta\in\Theta_s, \phi\in\Phi_s, \\ & (c5) \quad \mathbf{C^{(k)}} \succeq 0, \\ & (c6) \quad \zeta^{(k)}\mathbf{I}_{2L} - \mathbf{\Lambda}^{(k-1)^H}\mathbf{C}^{(k)}\mathbf{\Lambda}^{(k-1)} \succeq 0, \\ & (c7) \quad \zeta^{(k)} \leqslant \zeta^{(k-1)}. \end{cases} \tag{20}$$

Once $\mathbf{p}^{(k)}$, $\mathbf{Q}^{(k)}$ and $\zeta^{(k)}$ are found by solving (20), $\mathbf{\Lambda}^{(k)}$ can be obtained by seeking an $(2L+1)\times(2L)$ matrix with orthonormal columns such that $\zeta^{(k)}\mathbf{I}_{2L} \succcurlyeq \mathbf{\Lambda}^{(k)^\dagger}\mathbf{C}^{(k)}\mathbf{\Lambda}^{(k)}$. It was shown in [5] that choosing $\mathbf{\Lambda}^{(k)}$ to be equal to the matrix composed of the eigenvectors of $\mathbf{C}^{(k)}$ corresponding to its $2L$ smallest eigenvalues is the appropriate choice.

Accordingly, at each iteration of the proposed algorithm, we need to solve SDP, followed by an Eigenvalue Decomposition (EVD). Algorithm 1 summarizes the steps of the proposed iterative approach for solving (2). To initialize the algorithm, $\mathbf{\Lambda}^{(0)}$ can be found through the eigenvalue decomposition of $\mathbf{C}^{(0)}$, obtained from solving (20) with omitting constraints (c6) and (c7). Further, we terminate the algorithm when the convergence criterion, as specified in line 7 of Algorithm 1, is met. Further, to facilitate better understanding, we illustrate the main steps of Algorithm 1 in Fig. 2 using a flow diagram.

Algorithm 1 Proposed Method; 2D Antenna Array Placement For Beampattern Matching Design.

Inputs: η_1, η_2, γ, Γ, Θ_m, Θ_s, Φ_m, Φ_s, M, N and L.
Outputs: $\mathbf{p}_t^\star$, $\mathbf{p}_r^\star$ and $\mathbf{w}^\star$.
$k \leftarrow 0$;
Obtain $\mathbf{Q}^{(0)}$ and $\mathbf{p}^{(0)}$ by solving (20) with constraints (c6) and (c7) removed;
Compute $\mathbf{C}^{(0)}$ and its EVD;
Compute $\mathbf{\Lambda}^{(0)}$, composed of the $2L$ eigenvectors of $\mathbf{C}^{(0)}$ associated with its smallest $2L$ eigenvalues;
While $||\mathbf{p}_2 - \mathbf{p}_1||_F > \gamma$
    $\mathbf{p}_1 \leftarrow \mathbf{p}^{(k)}$;
    $k \leftarrow k+1$;
    Obtain $\mathbf{p}^{(k)}$, $\mathbf{Q}^{(k)}$ and $\zeta^{(k)}$ by solving (20);
    Compute $\mathbf{C}^{(k)}$ and its EVD;
    Compute $\mathbf{\Lambda}^{(k)}$, composed of the $2L$ eigenvectors of $\mathbf{C}^{(k)}$associated with its smallest $2L$ eigenvalues;
    $\mathbf{p}_2 \leftarrow \mathbf{p}^{(k)}$;
end While
$\mathbf{p}^\star = \mathbf{p}_2$;
Solve (25) Using CVX [29] for designing $\mathbf{w}^\star = \mathbf{w}$;
Outputs: $\mathbf{p}^\star = [\mathbf{p}_t^{\star T}, \mathbf{p}_r^{\star T}]^T$ and $\mathbf{w}^\star$.

Proposition 1 (*Convergence*). *The proposed iterative algorithm converges to at least a local minimizer of the optimization problem defined in* (11)

Proof. It readily follows from constraint (c7) in (20) that $\lim_{k\to\infty} \frac{|\zeta^{(k)}|}{|\zeta^{(k-1)}|} \leq 1$. This implies that $\zeta^{(k)}$ converges at least sub-linearly to zero [30]. Consequently, for any arbitrary small tolerance $\epsilon_1 > 0$, there exists an integer $\mathcal{I}_1$ such that $\zeta^{(k)} \leq \epsilon_1$ for $k \geq \mathcal{I}_1$. Utilizing this result and considering constraint (c6) in (20), it follows directly that,

$$\mathbf{\Lambda}^{(k-1)^H}\mathbf{C}^{(k)}\mathbf{\Lambda}^{(k-1)} \preccurlyeq \epsilon_1 \mathbf{I}_{2L}, \quad \text{for all } k \geq \mathcal{I}_1. \tag{21}$$

Now let $\rho_1^{(k)} \leq \rho_2^{(k)} \leq \cdots \leq \rho_{2L}^{(k)}$ denote the eigenvalues of $\mathbf{C}^{(k)}$ corresponding to its $2L$ smallest eigenvalues. According to [31, Corollary 4.3.16], the following inequality holds,

$$\text{Diag}([\rho_1^{(k)}, \rho_2^{(k)}, \ldots, \rho_{2L}^{(k)}]^T) \preccurlyeq \mathbf{\Lambda}^{(k-1)^H}\mathbf{C}^{(k)}\mathbf{\Lambda}^{(k-1)}. \tag{22}$$

Combining (21) and (22), it follows that $\text{Rank}(\mathbf{C}^{(k)}) \simeq 1$ for $k \geq \mathcal{I}_1$, which in turn indicates that $\mathbf{Q}^{(k)} = \mathbf{p}^{(k)}\mathbf{p}^{(k)^T}$ [5] for $k \geq \mathcal{I}_1$. This implies that $[\mathbf{Q}^{(k)}, \mathbf{p}^{(k)}]$, for any $k \geq \mathcal{I}_1$, is a feasible point for the optimization problem (11).

Additionally, by properly selecting η_2, there exists another integer $\mathcal{I}_2$ such that $\sum_{i=1}^{2L} h(\mathbf{p}_i^{(k)}) \leq \epsilon_2$ for $k \geq \mathcal{I}_2$ where $\epsilon_2 > 0$ is an arbitrarily small tolerance. Therefore, considering also the fact that $\zeta^{(k)} \leq \epsilon_1$ for $k \geq \mathcal{I}_1$, we conclude that $\mathbf{Q}^{(k)} = \mathbf{p}^{(k)}\mathbf{p}^{(k)^T}$, for any $k \geq \mathcal{I} = \max(\mathcal{I}_1, \mathcal{I}_2)$, is also a minimizer of

$$\sum_{\substack{\theta\in\Theta_m \\ \phi\in\Phi_m}} \left| \frac{\tilde{\mathbf{a}}^T(\theta,\phi)\text{vec}(\mathbf{Q}^{(k)})}{MN} - \Gamma(\theta,\phi) \right|^2. \tag{23}$$

These imply that $[\mathbf{Q}^{(k)}, \mathbf{p}^{(k)}]$ for $i \geq \mathcal{I}$ is at least a local minimizer of the optimization problem (11). This complete the convergence proof. □

Remark 2. After obtaining the optimum solution $\mathbf{p}^\star \in \{0,1\}^{(N_t+N_r)\times 1}$, we can easily reconstruct the transmit- and receive-array position vectors, i.e., $\mathbf{p}_t^\star \in \{0,1\}^{N_t\times 1}$ and $\mathbf{p}_r^\star \in \{0,1\}^{N_r\times 1}$, by splitting the vector $\mathbf{p}^\star$. Indeed, the first N_t entries of $\mathbf{p}^\star$ correspond to transmit array position vector, i.e., $\mathbf{p}_t^*$, and the next N_r entries to receive array position vector, i.e., $\mathbf{p}_r^*$.

Remark 3. The primary computational burden of the proposed algorithm at each iteration arises from two key operations: solving the SDP problem (20) and performing the EVD of matrix $\mathbf{C}^{(k)}$. Based on the number of constraints and decision variables in the SDP formulation (20), the computational complexity of solving the SDP problem using an interior-point method is approximately $\mathcal{O}(7(2L+1)^3+49(2L+1)^2)$ per

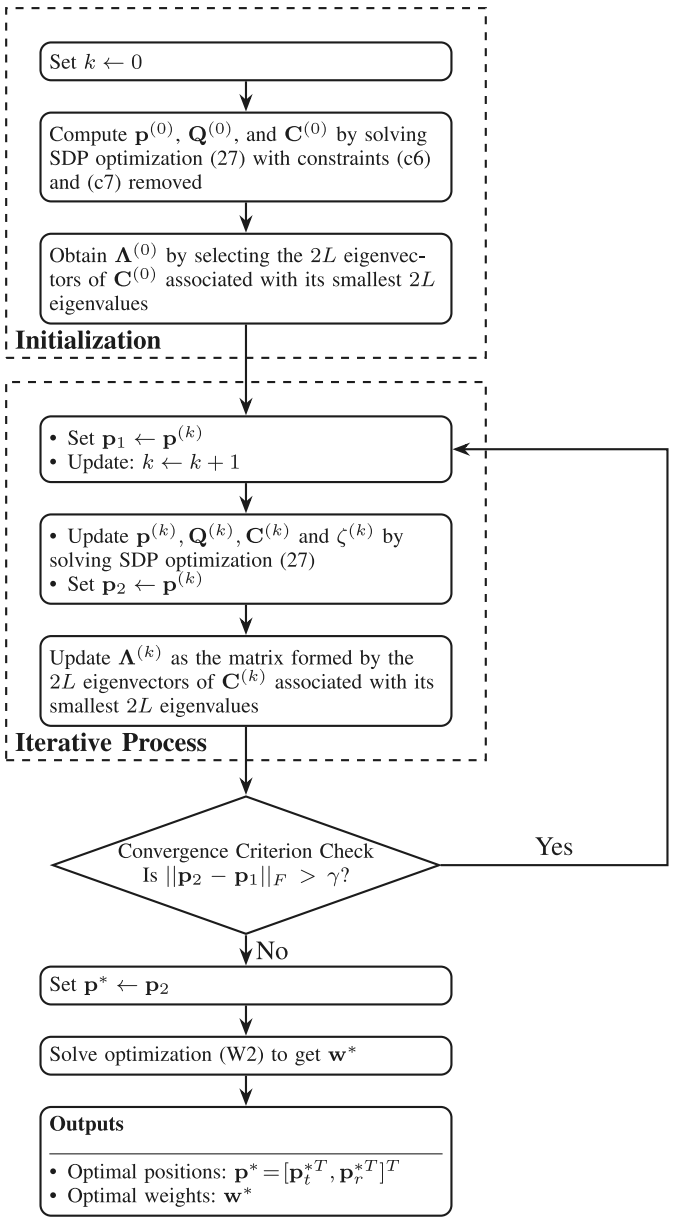

Fig. 2. Overview of the steps in Algorithm 1.

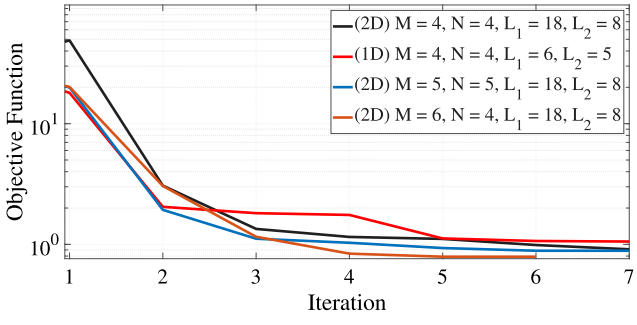

Fig. 3. Objective values of the proposed algorithm for different settings.

iteration [25]. Additionally, the computational complexity of the EVD operation required to update $\mathbf{\Lambda}^{(k)}$ is $\mathcal{O}((2L+1)^3)$. Therefore, the overall computational complexity of the proposed algorithm per iteration is approximately $\mathcal{O}(8(2L+1)^3 + 49(2L+1)^2)$.

After solving the nonconvex optimization problem and obtaining the sparse antenna array configuration, we achieve the desired angular resolution while adhering to the sidelobe constraints. However, although the array design is optimized, there is still room for improvement in the overall beampattern performance, specifically in terms of controlling SLLs with as little sacrifice to mainlobe resolution and the Processing Gain (PG) as possible. In practice, this is often achieved by introducing a weighting vector that adjusts the contributions of each antenna element in the array. This allows us to refine the beampattern further, improving the array's performance by reducing sidelobes while preserving the desired mainlobe characteristics to the greatest extent possible.

4. Weighting vector design for improving the array beampattern

In this section, we focus on designing a weighting/windowing vector to further enhance the beampattern of the array obtained from the previous optimization process [32–34]. The goal is to enhance the beampattern by preserving angular resolution and PG as much as possible, while simultaneously minimizing SLLs. Let $\tilde{\mathbf{a}}^{\star}(\theta,\phi) \triangleq \tilde{\mathbf{a}}_r^{\star}(\theta,\phi) \otimes \tilde{\mathbf{a}}_t^{\star}(\theta,\phi) \in \mathbb{C}^{4L^2}$ denote the manifold vector of the optimized array obtained from the solution in the previous section. The design problem for the weighting vector can now be formulated as,

$$\begin{cases} \min\limits_{\mathbf{w}} & \sum\limits_{\substack{\theta\in\Theta_m \\ \phi\in\Phi_m}} \left| \dfrac{\mathbf{w}^T\tilde{\mathbf{a}}^{\star}(\theta,\phi)}{\|\mathbf{w}\|_1} - \Gamma(\theta,\phi) \right|^2 \\ s.t. & \dfrac{\|\mathbf{w}\|_1^2}{\|\mathbf{w}\|_2^2} \geqslant t, \\ & \left| \dfrac{\mathbf{w}^T\tilde{\mathbf{a}}^{\star}}{\mathbf{1}^T\mathbf{w}} \right|^2 \leqslant \mu_2, \quad \forall\theta\in\Theta_s, \phi\in\Phi_s, \end{cases} \tag{24}$$

where $\mathbf{w}$ is the weighting vector. The objective function seeks to maintain the desired beampattern $\Gamma(\theta,\phi)$ in the mainlobe region. The first constraint ensures a certain level of Processing Gain (PG), while the second constraint limits the array SLLs. We note that the maximum achievable PG is MN, i.e., $t \leqslant MN$. This occurs only when all elements of $\mathbf{w}$ are identical, which corresponds to applying a rectangular window. Here the goal is to shape $\mathbf{w}$ such that the sidelobe level becomes a desired smaller value while the PG approaches MN. Without loss of generality, we can assume $\|\mathbf{w}\|_1$ is normalized to a constant, e.g., 1. Thus, the optimization problem (24) can be reformulated as,

$$\begin{cases} \min\limits_{\mathbf{w}} & \sum\limits_{\substack{\theta\in\Theta_m \\ \phi\in\Phi_m}} \left| \mathbf{w}^T\tilde{\mathbf{a}}^{\star}(\theta,\phi) - \Gamma(\theta,\phi) \right|^2 \\ s.t. & \|\mathbf{w}\|_1 = 1, \\ & \|\mathbf{w}\|_2^2 \leqslant \dfrac{1}{\gamma MN}, \\ & \left| \mathbf{w}^T\tilde{\mathbf{a}}^{\star} \right|^2 \leqslant \mu_2, \quad \forall\theta\in\Theta_s, \phi\in\Phi_s, \end{cases} \tag{25}$$

where $0 < \gamma \leqslant 1$ represents a scalar that should be as close to 1 as possible to attain the maximum PG. There is always a trade-off between γ and μ_2 as a higher γ leads to a higher value of μ_2. The optimization problem (25) is convex and can be efficiently solved using CVX [29]. This step is summarized in line 16 of Algorithm 1.

Remark 4. Although the proposed algorithm may be computationally expensive due to the use of AO and MM techniques, this computational burden occurs during the offline design phase of the chip and corresponding antenna array configuration. Once the design is finalized and the antenna array is manufactured, there is no need for further optimization, as the chip and array configuration remain fixed. Besides, $\mathbf{w}$ optimization described in this section, will give further flexibility to such designs.

5. Numerical results

In this section, we present numerical results to evaluate the performance of the proposed algorithm across various scenarios. Fig. 3 illustrates the convergence behavior of the objective function across iterations of Algorithm 1, under different configurations with varying array dimensions and sparsity levels in both 1D and 2D scenarios. As shown, the objective function decreases monotonically, confirming the convergence behavior of the proposed method, as established in Proposition 1.

The subsequent numerical and simulation results are divided into two parts, corresponding to the 2D and 1D SSA design cases. For the 2D case, we compare the performance of the designed 2D SSA using our proposed algorithm with that of the method introduced in [18], which, to the best of our knowledge, is the only existing work addressing the 2D SSA design problem. For the 1D case, we benchmark the performance of our proposed algorithm against both the method in [18] and the approach presented in [12], which is among the state-of-the-art techniques for 1D SSA design.

5.1. 2D antenna array configuration

In this part, we consider the design of a 2D antenna array to enable both azimuth and elevation angle estimation. We use 2D arrays with grid sizes set to half-wavelength spacing in our designs. The desired beampattern, depicted in Fig. 4(a), features 3 dB beamwidths of 6.8° and 15.2° in azimuth and elevation angles, respectively. In addition, the maximum sidelobe level is set to −9 dB within a FoV of $(-90°, 90°)$ in azimuth angles and $(-20°20°)$ in elevation angles. Achieving this conventionally requires a uniform 2D rectangular array with 144 virtual elements, which could arise from 18 physical transmit antennas and 8 physical receive antenna. The aim is to achieve such a beampattern using only 4 transmit and receive antennas, i.e., $M = N = 4$. This design provides a virtual array that is 89% sparser compared to the uniform 2D rectangular antenna array, resulting in significant computational savings. Further, this design requires 70% less physical transmit and receive antenna elements, which remarkably reduces the hardware costs.

The beampattern of the designed antenna array using the proposed algorithm is shown in Fig. 4(b). Moreover, Figs. 5(a) and 5(b) depict the azimuth and elevation cuts of the 2D beampattern of the designed antenna array, respectively. The designed sparse array's transmit and receive antenna configurations, along with the related virtual array, are shown in Figs. 6(a) and 6(c), respectively. As observed, the designed beampattern retains the mainlobe width and achieves SLLs of approximately −9.5 dB, demonstrating effectiveness of the proposed algorithm. Note that the grating lobes seen in Fig. 5(b) for the design array beampattern are due to the FOV design considerations and are outside the desired FoV.

Figs. 4 and 5 also compare the results with those obtained from the **TALA** algorithm [18]. It is observed that our proposed algorithm achieves lower SLLs (by approximately 7.5 dB) compared to the **TALA** algorithm. Furthermore, we can directly interleave the beampattern to design the antenna array structure, whereas in [18], the authors design the array to achieve only a specific virtual array configuration. Additionally, there is no control over the SLLs in the beampattern obtained from the **TALA** algorithm. This lack of control results in significantly high SLLs, reaching approximately −2 dB at azimuth angles of −20° and 20°, as observed in Fig. 5(a). Table 1 summarizes the comparison of key performance metrics between the antenna array designed using our proposed algorithm and that obtained from the **TALA** algorithm.

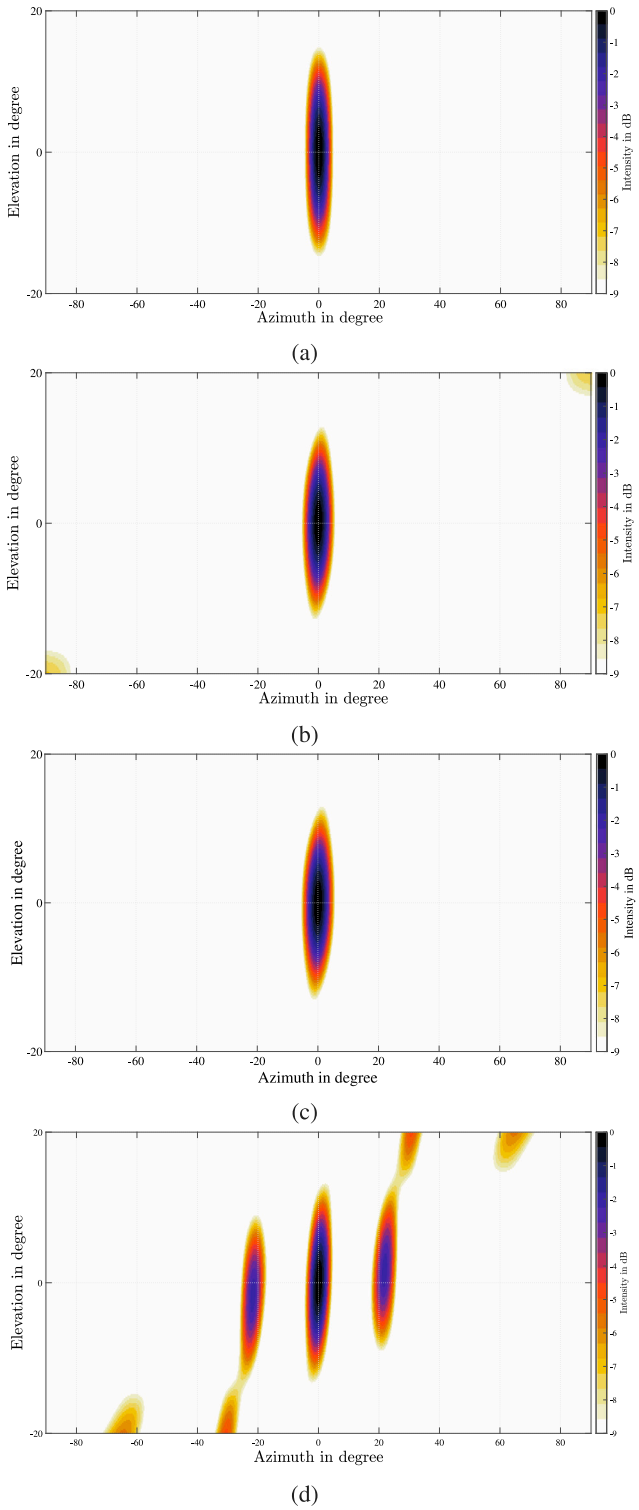

Fig. 4. (a) Desired and (b) designed 2D antenna array beampatterns; (c) beampattern of the designed array after applying array weighting; (d) designed beampattern obtained using the method in [18].

5.2. 1D antenna array configuration

As highlighted earlier in Remark 1, the proposed method can be readily adapted to the 1D SSA design with minor modifications. Accordingly, in this section, we evaluate its performance under a 1D configuration for both transmit and receive antenna elements. The goal is to achieve a beampattern with the 3 dB-beamwidth of 3.6° and the maximum sidelobe level of −10 dB within Field of View (FoV) of $(-90°, 90°)$ in azimuth direction using only 4 transmit and receive antennas, i.e., $M = N = 4$. Traditionally, to achieve such a 3 dB-beamwidth, a 30-element virtual uniform linear antenna array is required. This would arise from 6 physical transmit antennas and 5 physical receive antenna. This implies that our design provides a virtual array that is 47% sparser compared to the virtual uniform linear antenna array, enabling significant savings in computational resources. Further, this design requires 28% less physical transmit and receive antenna elements, significantly reducing the hardware costs.

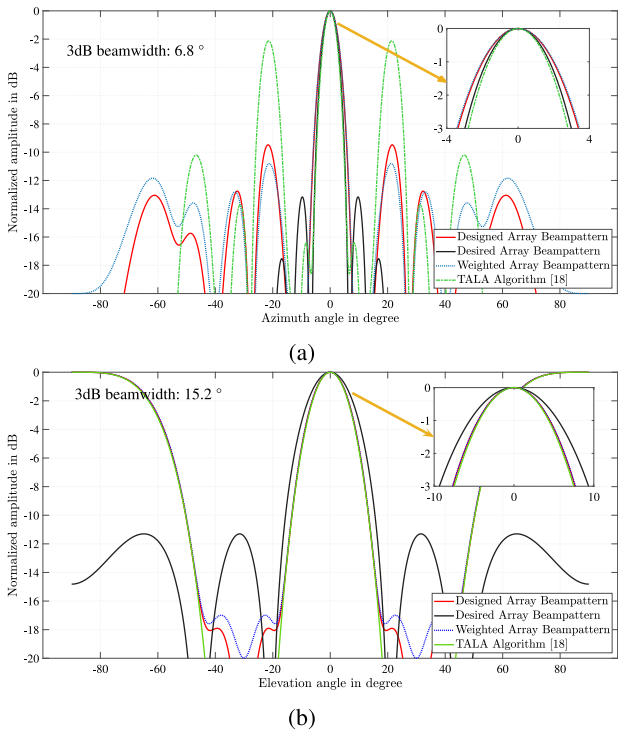

Fig. 5. Desired and designed antenna array beampatterns in (a) azimuth and (b) elevation, including the proposed design before and after array weight optimization, along with the beampattern obtained using the method in [18].

Table 1
Performance comparison of 2D SSA design.

Method	3 dB BW (Az.)	3 dB BW (El.)	SLL
Proposed	6.8°	15.2°	≈ − 9.5 dB
TALA [18]	6.8°	15.2°	≈ − 2 dB
Proposed (Weighted)	6.8°	15.2°	≈ − 10.8 dB

The beampattern of the designed antenna using the proposed algorithm is shown in Fig. 7. The results were obtained using scaling factors $\eta_1 = 1.6$, $\eta_2 = 1.3$, and termination parameter $\epsilon = 10^{-4}$. As seen, the designed antenna array provides almost 3 dB-beamwidth of 3.6° and the maximum sidelobe level of −10 dB as desired. Fig. 8(a) presents the configuration and positions of the transmit and receive antennas for the designed array. The corresponding virtual array, derived from the convolution of the transmit and receive antenna locations, is also illustrated Fig. 8(b).

A comparison of the array designs obtained by our proposed algorithm with those produced by the **TALA** algorithm in [18] and the CRLB-based approach in [12] is presented in Figs. 7 and 8. The results clearly demonstrate the superior performance of the proposed method. Specifically, the beampattern designed by our algorithm exhibits SLLs approximately 2 dB lower than those achieved by the **TALA** algorithm. This improvement is primarily due to the absence of sidelobe control in

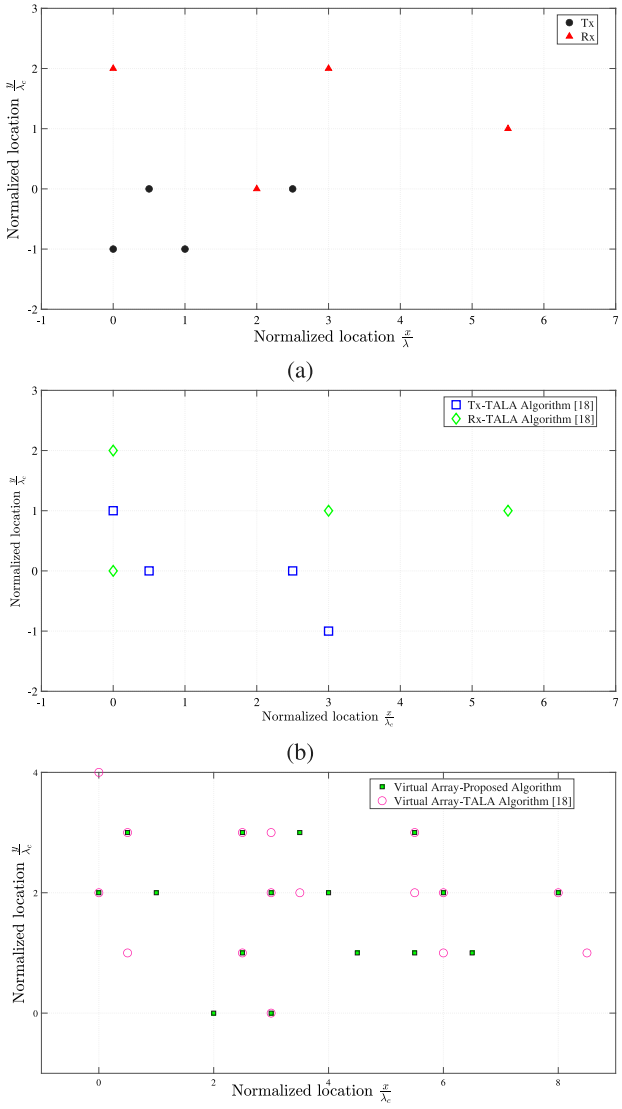

Fig. 6. Configuration and element positions of the designed (a) sparse array and (b) corresponding virtual array, obtained using the proposed algorithm, as well as the method in [18].

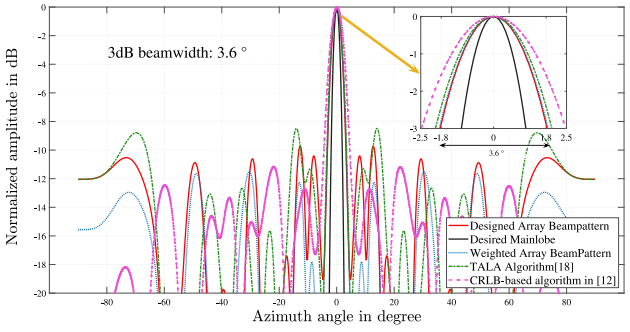

Fig. 7. Desired and designed 1D antenna array beampatterns, including the proposed design before and after array weight optimization, along with the beampatterns obtained using the methods in [12,18].

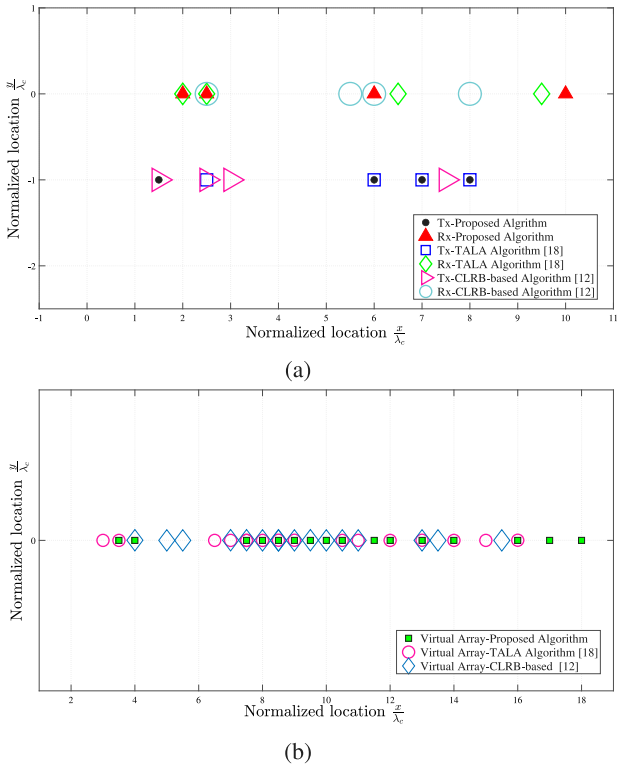

Fig. 8. Configuration and element positions of the designed (a) sparse array and (b) corresponding virtual arrays, obtained using the proposed algorithm, as well as the methods in [18] and [12].

Table 2
Performance comparison of 1D SSA design.

Method	3 dB BW (Az.)	SLL
Proposed	3.6°	≈ − 9.8 dB
TALA [18]	3.6°	≈ − 8.5 dB
CRLB-based [12]	5°	≈ − 11 dB
Proposed (Weighted)	3.6°	≈ − 11.5 dB

the array design formulation of [18], whereas our approach explicitly accounts for sidelobe suppression. Additionally, the 3 dB beamwidths of both methods are very similar.

In contrast, compared to the CRLB-based approach in [12], the proposed method achieves a significantly narrower 3 dB beamwidth (3.6° vs. 5°), which translates to enhanced angular resolution. Although the SLLs of the CRLB-based design are slightly lower, the trade-off in beamwidth performance highlights the advantage of our method in providing improved resolution while maintaining acceptable SLLs. Table 2 summarizes the comparison of key performance metrics between the antenna array designed using our proposed algorithm and those obtained from the TALA algorithm and the CRLB-based approach.

5.3. *Weighting vector design for beampattern improvement*

As discussed in Section 4, we formulated an additional optimization problem to design the array weight vectors, aiming to further enhance the beampattern of the sparse antenna array obtained in Section 3. The objective of this step was to reduce the maximum SLLs without affecting the mainlobe width. The resulting weighted array beampatterns for both the 1D and 2D cases are illustrated in Figs. 7, 5, and 4(c), respectively.

These results clearly show that the weighted array beampatterns successfully retain the desired mainlobe width while achieving noticeable sidelobe suppression, thereby enhancing the overall performance

of the array design obtained from Algorithm 1. Specifically, the maximum SLLs are reduced by approximately 2 dB in the 1D case and 1 dB in the 2D case, respectively. In particular, for the 1D design, this sidelobe reduction results in a beampattern that slightly outperforms the CRLB-based approach in [12] in terms of SLLs, while still maintaining a significant advantage in 3 dB beamwidth.

6. Conclusion

In conclusion, the paper presents a comprehensive investigation into the design of sparse planar antenna arrays for emerging mmWave MIMO radars. By leveraging high-frequency characteristics and spatial diversity, these radars offer enhanced capabilities for applications such as automotive radar and surveillance. The paper introduces an innovative algorithm that optimizes array placement to maintain equivalent characteristics of full antenna arrays with fewer transceivers, addressing the challenge of increased chip design costs and energy consumption. Through Majorization–Minimization algorithms and array weighting vectors, the proposed method effectively optimizes array beampatterns, reducing SLLs while preserving the mainlobe width and processing gain of the full array. We formulate the problem of joint transmit and receive array beampattern matching design and propose an optimization technique to tackle nonconvex NP-hard discrete optimization problems. The simulation results demonstrate the capability of the proposed method in designing sparse antenna arrays with desired characteristics. Overall, this work provides insights and paves the way for future research in sparse planar antenna array design for the 4D-Imaging mmWave MIMO radars.

CRediT authorship contribution statement

Saeid Sedighi: Writing – review & editing, Writing – original draft, Software, Methodology. **Nazila Karimian-Sichani:** Writing – review & editing, Writing – original draft, Software. **Bhavani Shankar M.R.:** Writing – review & editing, Supervision, Funding acquisition. **Maria S. Greco:** Writing – review & editing, Supervision, Funding acquisition. **Fulvio Gini:** Writing – review & editing, Supervision, Funding acquisition. **Björn Ottersten:** Writing – review & editing, Supervision, Funding acquisition.

Declaration of competing interest

The authors declare that they have no known competing financial interests or personal relationships that could have appeared to influence the work reported in this paper.

Data availability

No data was used for the research described in the article.

References

[1] I. Bekkerman, J. Tabrikian, Target detection and localization using MIMO radars and sonars, IEEE Trans. Signal Process. 54 (10) (2006) 3873–3883.
[2] J. Li, P. Stoica, MIMO Radar Signal Processing, John Wiley & Sons, 2008.
[3] A. Venon, Y. Dupuis, P. Vasseur, P. Merriaux, Millimeter wave FMCW RADARs for perception, recognition and localization in automotive applications: A survey, IEEE Trans. Intell. Veh. 7 (3) (2022) 533–555.
[4] J.-F. Hopperstad, S. Holm, The coarray of sparse arrays with minimum sidelobe level, 1998.
[5] E. Raei, S. Sedighi, M. Alaee-Kerahroodi, M.R. Bhavani Shankar, MIMO radar transmit beampattern shaping for spectrally dense environments, IEEE Trans. Aerosp. Electron. Syst. 59 (2) (2023) 1007–1020.
[6] C. Vasanelli, R. Batra, A.D. Serio, F. Boegelsack, C. Waldschmidt, Assessment of a millimeter-wave antenna system for MIMO radar applications, IEEE Antennas Wirel. Propag. Lett. 16 (2017) 1261–1264.
[7] Z. Cheng, Y. Lu, Z. He, Yufengli, J. Li, X. Luo, Joint optimization of covariance matrix and antenna position for MIMO radar transmit beampattern matching design, in: 2018 IEEE Radar Conference, RadarConf18, 2018, pp. 1073–1077.
[8] R.Z. Syeda, T.G. Savelyev, M.C. van Beurden, A.B. Smolders, Sparse MIMO array for improved 3D mm- wave imaging radar, in: 2020 17th European Radar Conference, EuRAD, 2021, pp. 342–345.
[9] Z. Haowei, X. Junwei, S. Junpeng, Z. Zhaojian, Antenna selection in MIMO radar with collocated antennas, J. Syst. Eng. Electron. 30 (6) (2019) 1119–1131.
[10] M. Deng, Z. Cheng, Z. He, Co-design of waveform correlation matrix and antenna positions for MIMO radar transmit beampattern formation, IEEE Sensors J. 20 (13) (2020) 7326–7336.
[11] E.K. Ghafi, S.A. Ghorashi, E. Mehrshahi, Reconfigurable linear antenna arrays for beam-pattern matching in collocated MIMO radars, IEEE Trans. Aerosp. Electron. Syst. 57 (5) (2021) 2715–2724.
[12] E. Tohidi, M. Coutino, S.P. Chepuri, H. Behroozi, M.M. Nayebi, G. Leus, Sparse antenna and pulse placement for colocated MIMO radar, IEEE Trans. Signal Process. 67 (3) (2019) 579–593.
[13] X. Wang, M. Amin, X. Cao, Analysis and design of optimum sparse array configurations for adaptive beamforming, IEEE Trans. Signal Process. 66 (2) (2018) 340–351.
[14] X. Wang, A. Hassanien, M.G. Amin, Dual-function MIMO radar communications system design via sparse array optimization, IEEE Trans. Aerosp. Electron. Syst. 55 (3) (2019) 1213–1226.
[15] S. Joshi, S. Boyd, Sensor selection via convex optimization, IEEE Trans. Signal Process. 57 (2) (2009) 451–462.
[16] M. Stolz, M. Wolf, F. Meinl, M. Kunert, W. Menzel, A new antenna array and signal processing concept for an automotive 4D radar, in: 2018 15th European Radar Conference, EuRAD, 2018, pp. 63–66.
[17] X. Wang, E. Aboutanios, M.G. Amin, Adaptive array thinning for enhanced DOA estimation, IEEE Signal Process. Lett. 22 (7) (2015) 799–803.
[18] N. Karimian-Sichani, M. Alaee-Kerahroodi, B.S. Mysore Rama Rao, E. Mehrshahi, S.A. Ghorashi, Antenna array and waveform design for 4-d-imaging mmwave MIMO radar sensors, IEEE Trans. Aerosp. Electron. Syst. 60 (2) (2024) 1848–1864.
[19] A.M. Elbir, K.V. Mishra, Y.C. Eldar, Cognitive radar antenna selection via deep learning, IET Radar, Sonar Navig. 13 (6) (2019) 871–880.
[20] X. Wang, W. Zhai, M.S. Greco, F. Gini, Cognitive sparse beamformer design in dynamic environment via regularized switching network, IEEE Trans. Aerosp. Electron. Syst. 59 (2) (2023) 1816–1833.
[21] A.M. Elbir, K.V. Mishra, Sparse array selection across arbitrary sensor geometries with deep transfer learning, IEEE Trans. Cogn. Comm. Netw. 7 (1) (2021) 255–264.
[22] X. Wang, M.S. Greco, F. Gini, Adaptive sparse array beamformer design by regularized complementary antenna switching, IEEE Trans. Signal Process. 69 (2021) 2302–2315.
[23] S. Wandale, K. Ichige, Design of sparse arrays via deep learning for enhanced DOA estimation, EURASIP J. Adv. Signal Process. 2021 (2021) 1–13.
[24] N.K. Sichani, M. Alaee-Kerahroodi, E. Raei, B.S.M. R., E. Mehrshahi, S.A. Ghorashi, MIMO virtual array design for mmwave 4D-imaging radar sensors, in: 2023 31st European Signal Processing Conference, EUSIPCO, 2023, pp. 1569–1573.
[25] S. Boyd, L. Vandenberghe, Convex Optimization, Cambridge University Press, 2004.
[26] S. Sedighi, M.R.B. Shankar, M. Soltanalian, B. Ottersten, Doa estimation using low-resolution multi-bit sparse array measurements, IEEE Signal Process. Lett. 28 (2021) 1400–1404.
[27] D.R. Hunter, K.L. Lange, A tutorial on MM algorithms, Amer. Statist. 58 (2004) 30–37, URL https://api.semanticscholar.org/CorpusID:228631.
[28] Y. Sun, P. Babu, D.P. Palomar, Majorization-minimization algorithms in signal processing, communications, and machine learning, IEEE Trans. Signal Process. 65 (3) (2017) 794–816.
[29] M. Grant, S. Boyd, CVX package, 2012, URL http://www.cvxr.com/cvx.
[30] J.R. Senning, Computing and estimating the rate of convergence, 2007.
[31] R.A. Horn, C.R. Johnson, Matrix Analysis, Cambridge University Press, 2012.
[32] W.P. du Plessis, Weighted thinned linear array design with the iterative FFT technique, IEEE Trans. Antennas and Propagation 59 (9) (2011) 3473–3477.
[33] S. Kumar, S. Raj, P. Sharma, A. Sharma, R. Gowri, Design of weighted circular array for 5G applications with fixed beam forming, in: 2018 5th International Conference on Signal Processing and Integrated Networks, SPIN, 2018, pp. 940–943.
[34] M.R. Sarker, M.M. Islam, M.T. Alam, M. Hossam-E-Haider, Side lobe level reduction in antenna array using weighting function, in: 2014 International Conference on Electrical Engineering and Information and Communication Technology, 2014, pp. 1–5.